MATERIALS FOR EFFICIENT HIGH-FLUX MAGNETIC BEARING ACTUATORS

M.E. Williams and D.L. Trumper

Dept. of Electrical Engineering
Univ. of N. Carolina at Charlotte
Charlotte, NC 28223

SUMMARY

Magnetic bearings have demonstrated the capability for achieving positioning accuracies at the nanometer level in precision motion control stages. This makes possible the positioning of a wafer in six degrees of freedom with the precision necessary for photolithography. To control the position of an object at the nanometer level, a model of the magnetic bearing actuator force-current-airgap relationship must be accurately obtained. Additionally, to reduce thermal effects the design of the actuator should be optimized to achieve maximum power efficiency and flux density. Optimization of the actuator is accomplished by proper pole face sizing and utilizing a magnetic core material which can be magnetized to the highest flux density with low magnetic loss properties. This paper describes the construction of a magnetic bearing calibration fixture designed for experimental measurement of the actuator force characteristics. The results of a material study that review the force properties of nickel-steel, silicon-steel, and cobalt-vanadium-iron, as they apply to magnetic bearing applications are also presented.

INTRODUCTION

Primarily, magnetic bearings are capable of applying forces and torques to a suspended object without rigidly constraining any of its degrees of freedom. The resolution of magnetic bearings is limited by sensors and control electronics, and not by the finish of a bearing surface. For these reasons, magnetic bearings appear to be ideal for performing wafer positioning in photolithography.

A theoretical model for the actuator force-current-airgap relationship can be derived from classical magnetic circuit theory. However, this is accurate only at very small airgaps and low flux densities. As the gap and the coil current increase, the actuator core saturates and the theoretical model is no longer effective. To obtain an accurate model, the actuator can be characterized for its force-current-airgap relationship. This characterization data can be linearized in real time and implemented in a digital control algorithm. A calibration fixture has been constructed to record the actuator force-current-airgap relationship throughout the useful range. Measurement data can then be stored as a three dimensional look-up table and linearized in real time to provide accurate control of the magnetic bearing over a wide range of airgaps.

An important consideration in the design of the magnetic actuators is the core material. Using the calibration fixture, various core materials can be evaluated for hysteresis, permeability, and saturation. Based on the results, the material that best fits the application criteria can be selected.

The actuators designed for a photolithography stage require the lowest possible hysteresis for all airgaps and sufficient force without excessive power requirements. Four identical test actuators were constructed with laminations cut from 49% nickel-steel, 80% nickel-steel, grain oriented silicon-steel, and Co-V-Fe. The characteristics of the test materials were determined and recorded as the airgap was varied from 80 to 650 μm.

This paper will briefly describe the magnetic levitation stage and the calibration fixture used to characterize the actuators. The method for optimizing the lamination pole face area will be presented. Finally an analysis of the core material properties and their effects on the performance of the actuators will be presented.

MAGNETIC BEARING PHOTOLITHOGRAPHY X-Y STAGE

The authors have previously reported on the design of a magnetic bearing stage for precision motion control[1,2,3]. The function of a stage for photolithographic systems is to align in six degrees of freedom a die site on a silicon wafer with the image plane of the lithographic lens. Although a previously reported magnetic bearing stage demonstrated proof-of-concept it did not possess the necessary range of motion to be directly applicable to photolithography systems.

An improved advanced stage that has the necessary range of motion and level of precision suitable for photolithography has been designed and is currently under construction. This next generation stage will provide 200 mm travel in the X-Y plane of the wafer allowing exposure over any portion of that area. For fine focusing the stage will provide 300 μm of travel normal to the wafer surface and milliradian rotations around three axes. One of the design objectives is to have the acceleration necessary to step and settle 20 mm in under 200 msec. At the die site the stage position must be maintained with a standard deviation better than 10 nm during the 300 msec exposure time. Magnetic bearings appear to be ideal for this application since the small rotational and focus motions can be provided without the need for additional fine stage mechanics. The design requirements have been fulfilled by a stage design that utilizes variable reluctance magnetic bearings to constrain five degrees of freedom, and a permanent magnet linear motor to position the stage 200 mm in the sixth degree of freedom (X). A conventional mechanical linear slide will be used to provide the necessary 200 mm of travel in the Y direction. This design increases power efficiency and yields better performance by capitalizing on the typical operation of a photolithography X-Y stage. Typical operation of a stage is to step in the X direction 10 - 20 times along a row of die sites, before a single step is made in the Y direction to the next row of die sites. Since the stage operation is dominated by X positioning, this mechanical-magnetic bearing stage design results in a simple magnetic bearing structure while simultaneously increasing the stage precision and throughput.

The advanced magnetic bearing stage will use three variable reluctance actuators each rotated by 90° contained in a common housing with four of these located at each corner of a 250 mm square platen. This configuration results in a total of twelve actuators as shown in Figure 1. The stage actuators are designed to have a nominal bearing airgap of 300 μm with displacements of $\pm$150 μm from the nominal. The actuators act on long laminated targets contained in the machine base and provide control in five degrees of freedom. To reduce the power dissipated, permanent magnets will be used to provide a DC lift to fully support the mass of the platen, enabling the actuators to be energized only for focusing control.

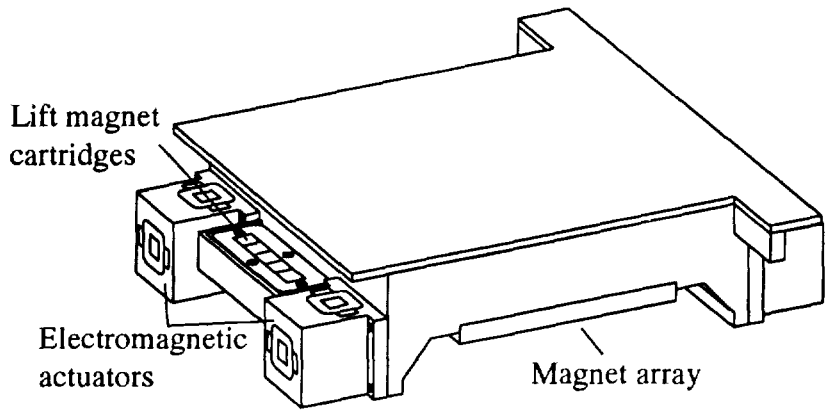

Figure 1: Advanced stage magnetic bearing suspended platen

To provide the long range X travel, a unique permanent magnet Lorentz type linear motor has been designed. The motor consists of a permanent magnet Halbach [4,5] array attached to the underside of the platen and a planar, ironless, six phase stator fixed in the machine frame. The magnet array uses four magnet blocks per period, with the magnetization axis rotating by 90° in each successive block. This array arrangement results in the fundamental field strength on one side of the array being increased by 1.4 over a conventional array and thus doubling the power efficiency of the motor. Figure 2 shows the finite element solution for a section of the magnet array. The arrows indicate the direction of magnetization. The motor design allows for a large area thermal path and the low motor height is compatible with the stage geometry.

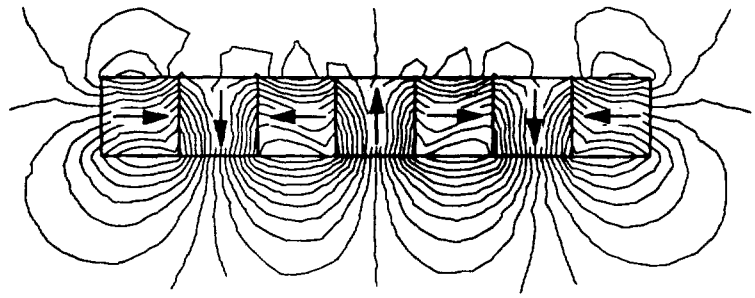

Figure 2: Single sided Halbach magnet array

The magnetic bearing as well as the linear motor will be controlled by a digital signal processor implemented on a VME bus chassis. Position feedback will be accomplished by capacitance gauging in the five actuator degrees of freedom to provide the controller with a true reading of the bearing airgap. Given the airgap and the desired force, the controller can linearize the bearing model and provide the required current. Laser interferometry will provide position feedback in the long travel X axis.

Further optimization is achieved through minimizing the platen mass without significantly sacrificing stiffness. The reduced mass will increase stage acceleration for a given input power. Having briefly covered the stage design the focus of the remainder of the paper is on the optimization and material selection for the variable reluctance actuators and the calibration fixture developed for this purpose.

ACTUATOR CALIBRATION FIXTURE

A test fixture has been developed to characterize the force of magnetic bearing actuators as a function of coil current and the target airgap. This fixture consists of a lightweight target platen constructed from composite materials mounted on to the fixture body through an extremely stiff silicon carbide gothic arch ball-and-groove coupling. This combination of high coupling stiffness and low platen mass results in a test fixture resonant frequency of 1.8 kHz, enabling the characterization of actuators at frequencies up to 1kHz. The calibration fixture was developed with the following design objectives:

- Measure the actuator force at airgaps ranging from 10 to 1000 μm.
- Achieve a peak force capability on the order of hundreds of newtons.
- Permit the adjustment of the target separation gap.
- Separation of the force and metrology loop to accurately measure the target airgap.
- Allow the testing of a variety of actuator sizes interchangeably.

The following section describes the mechanical design of the fixture and how the objectives were achieved. The actuator test procedure is described followed by the results of force testing the various magnetic actuator materials.

Calibration Fixture

The magnetic bearing calibration fixture consists of an aluminum fixture body and platform, three adjustable support columns with ball-and-groove kinematic couplings, three capacitance probes, and a target platen as shown in Figure 3. The electromagnet consists of E-shaped stacked laminations with a single coil surrounding the central leg and housed within a mounting cartridge. The cartridge is mounted inside the test fixture body so that its pole face is exposed upward toward the target platen. A laminated target made from the same material as the E-core is attached to the underside of the target platen. Located at 120 degree intervals around the perimeter of the fixture body are the three support columns, each consisting of a kinematic ball/groove coupling mounted on top of a piezoelectric load cell. The columns are supported by a shaft clamped to the fixture body and can be locked in position once located. The hemisphere mounted to the top of each load cell makes two points of contact in each of three grooves, thus the three couplings provide exactly six constraints on the six platen degrees of freedom. If properly designed this type of kinematic coupling, commonly referred to as a Maxwell mount, exhibits sub-micron positional repeatability. The micrometer head pushes against the end of the support shaft and is used to adjust the height of the platen above the electromagnet. The load cells measure the attractive force between the electromagnet and the target platen. Three capacitance probes mounted at the top perimeter of the fixture body are used to sense the distance between the electromagnet and three datum pads on the target platen. The coil is driven by a linear power amplifier capable of driving the electromagnets into saturation.

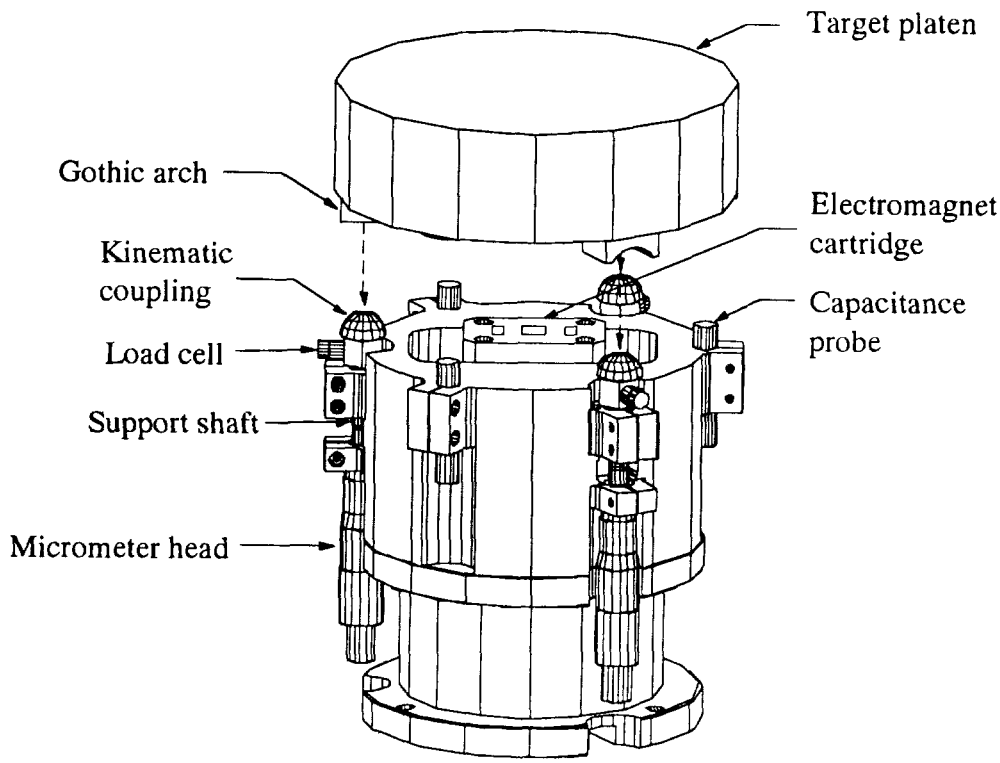

Figure 3: Magnetic bearing calibration fixture.

Actuator Calibration Procedure

Characterization data provides a 3-D matrix of force versus current, parametric on airgap format. In a real time control algorithm the coil current is interpolated from this data from the target airgap and the desired actuator force. The actuator force versus current curves are recorded for airgaps ranging from 50 - 650 μm in 50 μm increments. Data collection is performed on a 386 based PC and a block diagram of the complete calibration facility is shown in Figure 4.

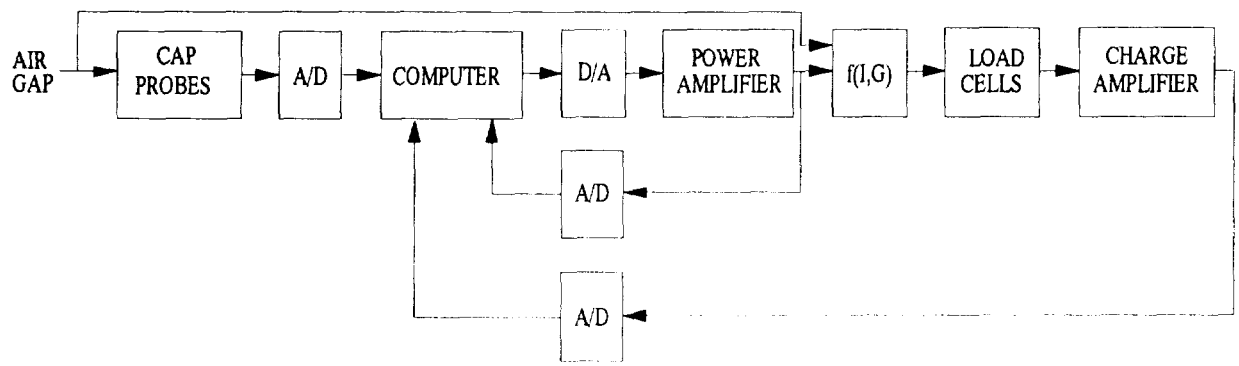

Figure 4: Magnetic bearing calibration procedure block diagram.

The airgap is manually set using the micrometer heads to position the platen. The airgap is determined from the capacitance gauges and fed back to the computer through analog to digital converters. When the desired airgap is set an automated data collection procedure is initiated.

The computer provides a signal to the power amplifier through the digital to analog converter that ramps the coil current up to a maximum of 1.5 amps and then returns to zero at the same rate. This triangular current input to the electromagnet results in a force at the target platen which transmits through the load cells and is monitored by the computer through an analog to digital converter. The airgap, force, and current are recorded in a data file after which the airgap is readjusted and the procedure repeated.

TEST ACTUATOR CONSTRUCTION AND SIZING

Selection of the core material is an important consideration in the design of high precision magnetic bearing actuators. A good material will possess low magnetic loss and coercive force but also be capable of high flux densities for low coil currents. General information about a material can be obtained from the B-H curve, but specific material performance for a given geometry of an electromagnetic actuator needs to be evaluated experimentally.

The four core materials considered were 49% nickel/steel alloy, 84% nickel/steel alloy, Co-V-Fe, and silicon steel. With the exception of the Co-V-Fe material the EI lamination pairs were obtained commercially . The Co-V-Fe EI laminations were custom laser cut and heat treated locally.

Four nominally identical actuators were fabricated using 0.014" laminations cut from these four materials. The most efficient configuration for the actuator is a lamination in the shape of an E with a single coil surrounding the central leg of the core. A single central coil is the shortest average coil length that will fill the core window. The shortest possible coil length is desirable in order to minimize resistance for a given number of amp-turns. A 240 turn coil wound with 22 awg magnet wire was used. Although a cut-core can be magnetized to higher flux densities, for our application laminations were the most economical means of obtaining a limited volume of material. Unlike a cut-core, while traversing through the back of the E lamination, the flux will be perpendicular to the direction of magnetization which has poor magnetic properties. Co-V-Fe has no preferred grain orientation and therefore E laminations will have the same magnetic properties as the more efficient cut-core [6].

The actuator target consisted of a laminated stack of I cores of the same material as the actuator and was tested as a pair. The surface of the target and the pole face of the actuator were both surface ground to ensure a reasonably flat and therefore consistent airgap.

In addition to the core material, the lamination size can be optimized for power. The dimensions of the core lamination can optimize force by sizing the pole face area in relation to the core length and height. Thus, for an optimum square pole face area the maximum force can be obtained for a given power level. The overall length and height of the core lamination are selected to place the operating point at nominal standoff in the middle, or most nearly linear region of the B-H curve of the core material.

The actuator force can be expressed in terms of the pole width and core window area. From magnetic circuit theory we define the relation for actuator force as

$$F = \frac{\mu_o A_p N^2 i^2}{4g^2} \tag{1}$$

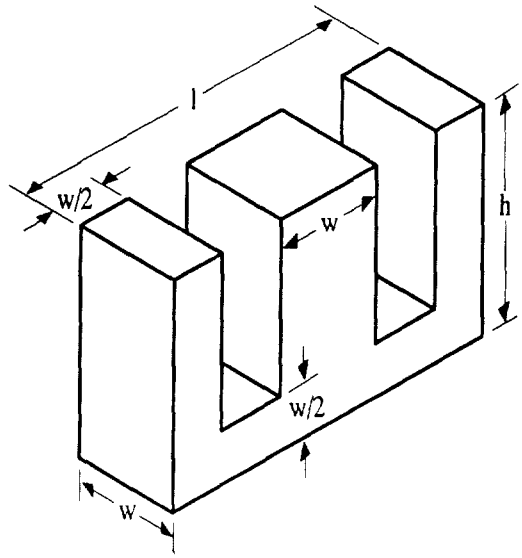

Figure 5: Electromagnet core sizing.

Since actuator power, $P = i^2R$ we obtain the force-power relation

$$F = \frac{\mu_o A_p N^2 P}{4g^2 R} \tag{2}$$

where A_p is the pole face area, N is the number of coil turns, and g is the actuator airgap. Assuming a square pole face, and realizing that the number of coil turns is equal to the area of the core window multiplied by a packing factor constant, we can reduce N to the window area in terms of the pole face width and lamination length and height. The packing factor is a scaling term and can therefore be eliminated.

$$N = A_w = 2w^2 - (4h + l)w + 2hl \tag{3}$$

If the average coil turn diameter is located in the middle of the core window, the average turn length will then be approximately equal to $2l$. Realizing that the coil resistance is the product of the average turn length, the number of turns, and a resistance constant per unit length, we can eliminate the scaling constants and express the coil resistance as

$$R = lA_w \tag{4}$$

Substituting equation (3) and equation (4) into equation (2), and eliminating all scaling constants including constant power, we establish a unit force function expressed in terms of the lamination dimensions. Since we are concerned with maximizing the function and not with the magnitude of the force and power, we can eliminate the terms that have no dependance on the lamination dimensions.

$$F_u = 2w^4 - (4h + l)w^3 + 2hlw^2 \tag{5}$$

Solving

$$\frac{\partial F_u}{\partial w} = w(8w^2 - 3(4h + l)w + 4hl) = 0 \tag{6}$$

will result in a pole face width, w, that will provide the maximum force for a given lamination length and height. Any system of units for length can be used. The commercially obtained EI pair used was selected based on this analysis and is reasonably close to the optimum pole face size. For the optimized E core the total stage power dissipation for a lateral acceleration of one half the force of gravity is calculated to be approximately 1.5 watts. This type of stage acceleration requires six actuators to be energized: two will provide accelerating force and the remaining four will offset any torques that result from moments about the center of gravity.

CORE MATERIAL FORCE RESULTS

The test actuators were characterized for airgaps ranging from 80 - 650 μm and the resulting curves are shown in Figures 6 to 9. In magnetic bearings which convert electrical power into mechanical power, high flux density materials offer the advantage of reduced volume and lighter weight. This is especially important in our magnetic levitation stage where the actuators are contained on the suspended platen. For precision control of a suspended platen, it is also essential that the material have low magnetic losses to reduce hysteresis. A material with higher losses and coercive force will introduce errors into the actuator real-time linearized model.

The Co-V-Fe material demonstrated extremely high flux concentrations, but exhibited higher electromagnetic losses and coercive force than are acceptable for our application. The losses exhibited are contrary to the material B-H curve and are probably attributed to the heat treatment which was performed locally. This material was tested both with and without heat treatment. The flux density of the material without heat treatment is approximately 10% of the properly annealed flux density. The Co-V-Fe material is considerably more expensive than other materials, but is a good value if one considers the flux per unit weight. Grain oriented silicon-steel exhibits the best value in flux per unit cost. This material is capable of high flux densities, but has more magnetic losses than are desirable. The nickel-steel alloys both have very low magnetic losses, but the permeability of 80% nickel-steel is reduced significantly and the material cannot produce the necessary force. The best combination of low magnetic losses and high force for our precision magnetic bearing is the 49% nickel steel alloy. The expected operating region of the actuators will be with airgaps between 150 - 450 μm and an excitation current of less than 1 amp. In this region the losses are negligible and the force-current-airgap relationship is very nearly linear.

CONCLUSIONS

This paper has introduced a precision motion control magnetically levitated stage and some aspects of the stage optimal design have been presented. The magnetic bearing calibration test fixture used to experimentally measure the force-current-airgap relationship was presented including its construction and test procedure. The force-current-airgap relationship for various magnetic materials was experimentally measured and a core material was selected based on the analysis.

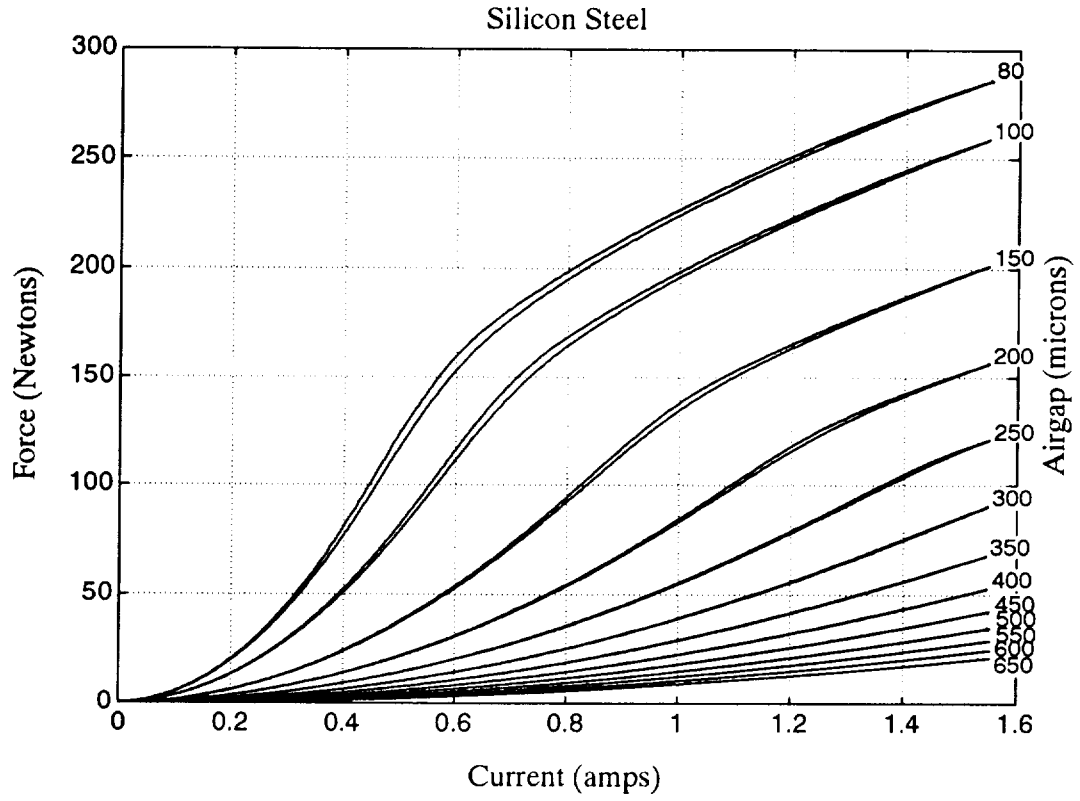

Figure 6: Silicon-steel force curves.

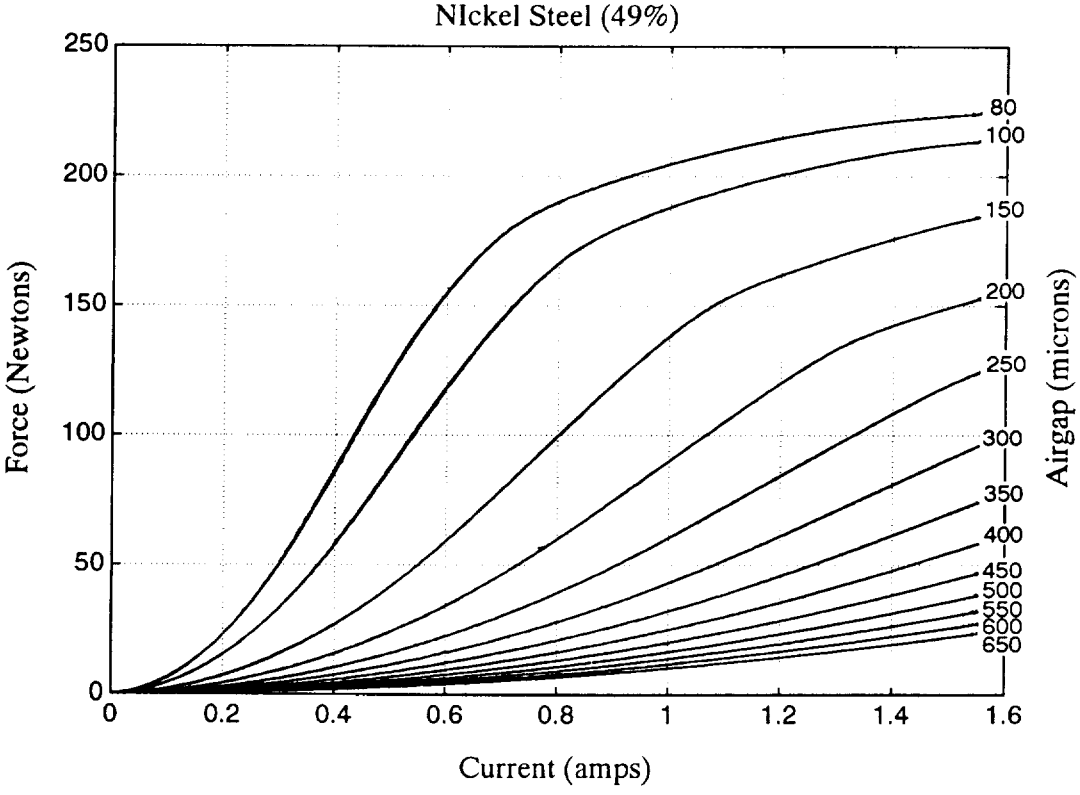

Figure 7: 49% Nickel-steel force curves.

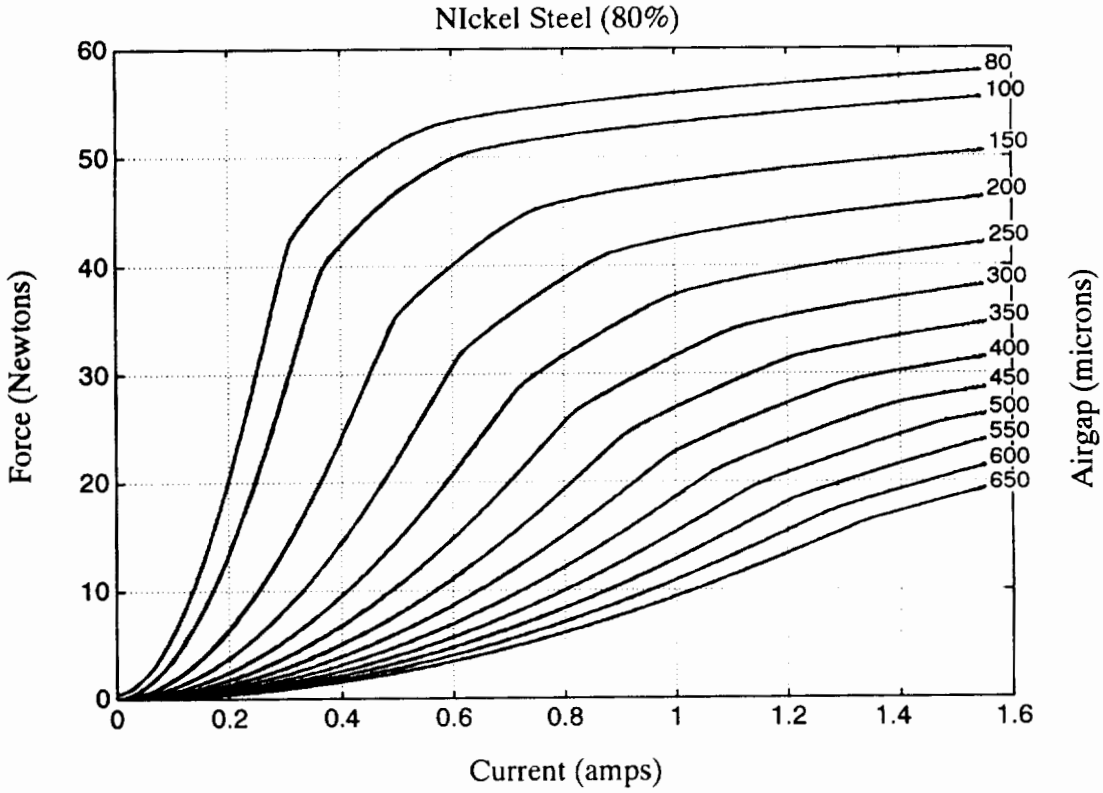

Figure 8: 80% Nickel-steel force curves.

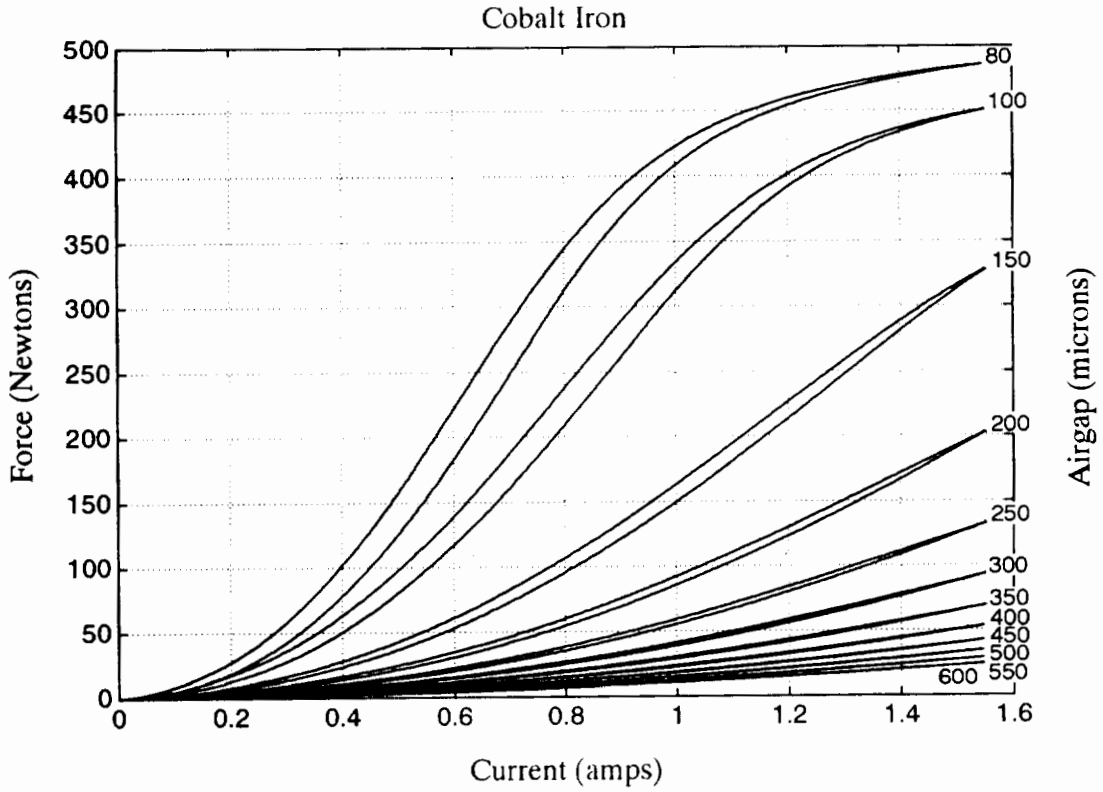

Figure 9: Co-V-Fe force curves.

References

[1] Trumper, D.L., "Magnetic Suspension Techniques for Precision Motion Control," Ph.D. Thesis, Dept. of Elec. Eng. and Comp. Sci., M.I.T., Camb., Mass., Sept., 1990.

[2] Trumper, D.L., and Slocum, A. H., "Five-Degree-of-Freedom Control of an Ultra-Precision Magnetically-Suspended Linear Bearing," NASA Workshop on Aerospace Applications of Magnetic Suspension Technology, NASA Langley Research Center, Hampton, VA, Sept. 25–27, 1990.

[3] Trumper, D.L., and Queen, M.A., "Precision Magnetic Suspension Linear Bearing," NASA International Symposium on Magnetic Suspension Technology, Aug. 19–23, 1991.

[4] Halbach, K., "Design of Permanent Multipole Magnets with Oriented Rare Earth Cobalt Material," Nuclear Instruments and Methods, 169, 1980, pp. 1–10, North-Holland Publishing Co.

[5] Halbach, K., "Physical and Optical Properties of Rare Earth Cobalt Magnets," Nuclear Instruments and Methods, 187, 1981, pp. 109–117, North-Holland Publishing Co.

[6] Finke, G., "Materials for High Flux Devices," Magnetic Metals Company, Camden, New Jersey.